Synthesis of Zn(II) and Co(II) Complexes with a Schiff Base Derived from Malonic Acid Dihydrazide for Photo-Stabilizers of Polystyrene

Rehab Ghalib Hammoda and Naser Shaalan*

Department of Chemistry, College of Science for Women, University of Baghdad, Baghdad 10071, Iraq

* ***Corresponding author:***

email:
naserds_chem@csw.uobaghdad.edu.iq

Received: April 8, 2023
Accepted: April 26, 2023

DOI: 10.22146/ijc.83730

Abstract: *In this study, novel Schiff base complexes with Zn(II) and Co(II) ions were successfully synthesized. The malonic acid dihydrazide was converted into the Schiff base ligand by combining it with 1-hydroxy-2-naphthaldehyde, and the last step required reacting it with the appropriate metal(II) chloride to produce pure target complexes. The generated complexes were thoroughly characterized using FTIR, ^{1}H-NMR, ^{13}C-NMR, GC-mass, and UV-Vis spectroscopies. In order to photo-stabilize polystyrene (PS) and reduce the photodegradation of its polymeric chains, these chemicals have been used in this work. The efficiency of the generated complexes as photo-stabilizers was evaluated using a variety of techniques, including FTIR, weight loss, viscosity average molecular weight, light and atomic force microscopy, scanning electron microscopy (SEM), and energy dispersive X-ray (EDX) mapping. These tests corroborated each other and demonstrated how effectively new compounds stabilize PS photographs. As a result, compared to blank PS, they reduce the photodegradation of PS films containing these complexes after 300 h of exposure to UV radiation with a wavelength of 313 nm. Also, it has demonstrated how effective the cobalt complex is as a photo-stabilizer. The highly conjugated systems in these chemicals are to blame for this.*

Keywords: *photodegradation; malonyl dihydrazide; photo-stabilization; polystyrene; Schiff base complexes*

■ INTRODUCTION

Due to its distinctive qualities, polystyrene (PS) is regarded as one of the most significant plastics. It can withstand many sorts of solvents, acids, and bases and is highly affordable, flexible, durable, light, and transparent. Additionally, it is synthesized in a variety of shapes, including solid and foam. PS is ideal for usage in a variety of applications, including packaging, labeling, and varied technical requirements [1-2]. Plastic polymeric materials are employed in a variety of applications, including organic electronics, polymeric light-emitting diodes (PLED), transistors, sensors, and solar cells, as well as anticorrosive coatings for metals [3].

UV light exposure to polymer chains causes the chemical structure of the polymer to photodegrade by producing free radicals. This causes covalent connections within the polymer structure to break or form new ones [4]. All of these chemical alterations will cause changes in the PS material's physical, mechanical, optical, and morphological characteristics, such as cracking, staining, paint layer solidification, and altered solubility properties [5]. Because it contains UV light, which has wavelengths within the dissociation energy of many organic polymeric materials, the sun's light is thought to be the primary cause of the photodeterioration of PS materials used outdoors [6].

In the presence of oxygen molecules and sunlight, polystyrene polymer chains undergo an oxidative process. It mostly results in polymer chain breaks or new cross-links being formed inside the polymer structure [7]. Typically, the polymer moieties in PS absorb photons to begin the process of photodegradation. Thus, the energy of the photons that were absorbed was sufficient to dissolve the covalent bonds that held the polymer chains together and create a free radical, which is known as the first stage in the breakdown of the polymer chains [8].

The chemical makeup of the polymer chain can be changed to increase the plastic polymer's photostability.

Even though combining UV absorber chemicals and/or other types of amines as photo stabilizers has demonstrated outstanding plastic protection, this fundamental technique is extremely seldom employed [9]. Organic UV stabilizers have been employed for a very long time to improve the photostability of polymers [10]. However, they are susceptible to degradation and transference inside the polymer chains themselves. Using them in large doses might have negative effects on safety. Numerous studies have utilized a variety of additives, including aromatics [11], Schiff bases [12], and organometallic compounds [13], to stabilize plastic polymer materials against photodegradation. Here, the synthesis, characterization, and effect of the new Schiff base complexes on the features and chemical structure of polystyrene films were described.

■ EXPERIMENTAL SECTION

Materials

The chemicals used in this study were diethyl malonate (Sigma Aldrich, 99%), hydrazine monohydrate (Sigma Aldrich, 99%), 1-hydroxy-2-naphthaldehyde (Sigma Aldrich, 98%), absolute ethanol (BDH, 99%), $CoCl_2 \cdot 6H_2O$ (BDH, 99%), $ZnCl_2$ (BDH, 98%), and polystyrene (Sigma Aldrich) from Gillingham, UK.

Instrumentation

The carbon, hydrogen and nitrogen contents were determined by Euro Vector EA 3000 A, and FTIR spectra were recorded on a Shimadzu FTIR-8100 spectrometer. ^{1}H-^{13}C-NMR spectra of the ligand (L) were measured in d_6-DMSO solvent using TMS as an internal standard on a Bruker 300 MHz. Using UV-1650 PC Shimadzu spectrophotometer were measured the electronic spectra at 25 °C. Electrical conductivity measurements of the complexes were recorded at 25 ± 2 °C for a 1×10^{-3} M solution of the samples in DMF using a Philips PW-digital conductivity meter. Magnetic susceptibility results were also obtained at 25 °C in the solid state by applying Gouy balance. The molecular weight of the prepared ligand was determined by a GCMS-QP2010 PLUS; DI analysis Shimadzu, Japan, spectrometer in the laboratory of the University of Samarra. Moreover, all melting point results were recorded on Gallen Kamp melting apparatus at the College of Science for Women, University of Baghdad. PS films were subjected to radiation using an accelerated weather-meter QUV tester that was purchased from Q-Panel Corporation, at 25 °C, and a wavelength of 365 nm (6.43 10^9 ein dm^{-3} s^{-1}). (USA, Homestead, Florida). Atomic force microscopy (AFM) was used to investigate the surface of PS films using Veeco equipment (Plainview, NY, USA). Scanning electron microscopy (SEM) of the PS surface was performed using an Inspect S50 microscope (FEI Corporation, Czechia, Czech Republic) and an accelerating voltage of 15 KV. The Meiji Techno Microscope was used to take minuscule images of the PS surface in Tokyo, Japan. PS films were placed using 0.6 mm thick aluminum plate supports, and a Digital Vernier Caliper 2610A micrometer (Vogel GmbH, Kevelaer, Germany) was used to measure the thickness of the films (approximately 40 μm) (Q-Panel Company, Homestead, FL, USA). Look for signs of accelerated UV weathering. With the aid of an accelerated weather meter QUV tester from Philips, Saarbücken, Germany, PS films were subjected to QUV radiation at 25 °C. The films were exposed for 300 h continuously to UV light with a wavelength of 313 nm and an intensity of 1.052×10^{-8} ein dm^{-3} s^{-1}. Using a Digital Vernier Caliper 2610A Micrometer, Polymeric Film Thickness was Measured (Vogel GmbH, Kevelaer, Germany).

Procedure

Preparation of polystyrene films

Polystyrene (1.0 g) was dissolved in 16 mL of tetrahydrofuran (THF), and the mixture was constantly agitated for 1 h at room temperature to produce PS films. The produced metal complexes(II) were added to the PS of THF solution at a weight proportion of 2% (per polymer weight), and the mixture was agitated for an additional hour to ensure that the metal complexes(II) were completely dissolved and the mixture was homogeneous. After that, the excess THF was eliminated from the mixture by putting it on glass plates

of the same size and allowing it to evaporate there for 24 h. Plate thickness is measured using micrometers of this type (2610A), and one approach is to attach cardboard sheets to the target plates and punch holes in them that are 3 × 2 cm in size.

Irradiation by UV light

It is a technique to assess the impacts of utilizing plastic materials outside following extended exposure to UV or solar radiation (for months or years). The created polymeric films were fastened to a support plate for UV-B 313 light exposure. This stand has a 0.6 mm thickness and is made of aluminum. Constant pressure and temperature were used for testing the films.

PS films' photostability is evaluated using FTIR

An FTIR 8300 Shimadzu spectrophotometer was used to investigate the efficacy of using synthetic compounds as photo-stabilizers to slow down the degradation of PS films. This method was used to monitor the development and growth of polyene and carbonyl groups. Eq. (1) is used to determine the hydroxyl index (I_{OH}) and carbonyl index ($I_{C=O}$) of plain PS, and PS doped with additives.

$$I_s = \frac{A_s}{A_r} \quad (1)$$

Hence for the peak absorption intensity of the functional group, A_s is used, whereas A_r is used for the reference group. I_s, on the other hand, refers to the functional group index [14].

Test of the photostability of PS films using a diet plan

Weighing was done on the polymeric PS films used in this process both before and after UV exposure. This method was carried out for both blank and mixed PS films, and the PS weight reduction was calculated using Eq. (2).

$$\text{Weight loss } \% = \frac{W_0 - W}{W_0} \times 100 \quad (2)$$

Before radiation exposure, the PS film weighed W_0, and after radiation exposure, the PS film weighed W [15].

Calculating the average molecular weight of the PS polymeric sheets (M_V)

The average molecular weight (M_V) of PS films before and after irradiation, as well as for blank and mixed PS films, may be calculated by measuring the viscosity of the polymer. The viscosity of PS with and without synthesized complexes was measured at room temperature using an Ostwald U-tube viscometer with THF as the solvent. MV denotes the average molecular weight of PS. Eq. (5) was used to obtain the average molecular weight of PS [16], whereas Eq. (4) was used to estimate the intrinsic viscosity [η].

$$[\eta] = \frac{\left[2\left(\eta_{sp} - \ln \eta_{rel}\right)\right]^{\frac{1}{2}}}{c} \quad (4)$$

$$[\eta] = 1.63 \times 10^{-2} M_v^{0.766} \quad (5)$$

In addition, Eq. (6) was used to estimate the specific viscosity (η_{sp}), and Eq. (7) to estimate the relative viscosity (η_{rel}).

$$\eta_{sp} = \eta_{re} - 1 \quad (6)$$

$$\eta_{re} = \frac{t}{t_0} \quad (7)$$

As a result, the polymer solutions' flow time is given by t, while the solvent's flow time is given by t_0 [17].

Synthesis of malonic acid dihydrazide

Making malonic acid dihydrazide is the first step in the ligand synthesis procedure, as described here. At room temperature, 10 g of diethyl malonate (0.062 mol) was dissolved in 10 mL of ethanol and stirred. Add dropwise of aqueous hydrazine (10 g, 0.124 mol) with continuous stirring followed by 6 h of refluxing the reaction before stopping and allowing it to cool to room temperature. The precipitate was washed with dry ether and methanol after the generated residue was filtered. A white precipitate with an 80% yield (7.1 g) was produced by recrystallizing the product in absolute ethanol at a temperature of 159 °C. This illustrates the manufacture of malonic acid dihydrazide [18] in Scheme 1.

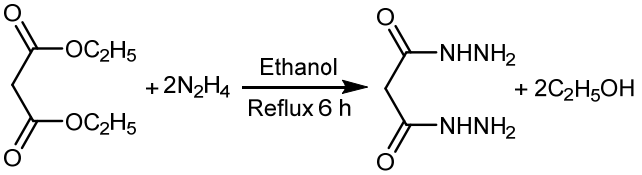

Scheme 1. Preparation of Malonic acid dihydrazide

Synthesis of a Schiff base ligand

Malonic acid dihydrazide solution (1.0 g, 0.0075 mol), in 10 mL of methanol was produced. Slowly while stirring, 2-hydroxy-1-naphthaldehyde (2.6 g, 0.015 mol) was added. The reaction mixture was then given a final addition of a few drops of glacial acetic acid. The combination was allowed 5 h to react in a reflux environment, at which point a glossy yellow precipitate was generated. This precipitate was recovered by filtering, cleaning, and recrystallizing in hot ethanol. See Scheme 2 for the reaction scheme. The product was dried over anhydrous $CaCl_2$ in a vacuum to provide 80% (2.88 g) yield, m.p. 230–234 °C.

Synthesis of Schiff base metal complexes

The zinc complex was synthesized by dissolving zinc chloride dehydrate (0.2 g, 0.001 mol) in 10 mL methanol and dissolving the synthesized ligand (0.5 g, 0.001 mol) in 10 mL methanol with continuous stirring for about 10 min and adding a few drops of DMF to complete solubility, followed by adding the solution of the dissolved metal salt onto a solution of the dissolved ligand in the mole ratio 1:1 of metal:ligand. In order to precipitate, the mixture was agitated under reflux for 5 h. The colorful complexes were filtered apart, cleaned with methanol, recrystallized, and allowed to dry for 24 h at room temperature. Cobalt complex ($CoCl_2{\cdot}6H_2O$) was prepared using the same procedure as shown in Scheme 3 with a good percentage yield see Table 1.

■ RESULTS AND DISCUSSION

Two steps were taken to synthesize the ligand. Diethyl malonate and two moles of aqueous hydrazine monohydrate were initially combined to create malonic acid dihydrazide. By recrystallization from absolute ethanol, the raw product was purified. Two moles of 2-hydroxy-1-naphthaldehyde were added to the pure

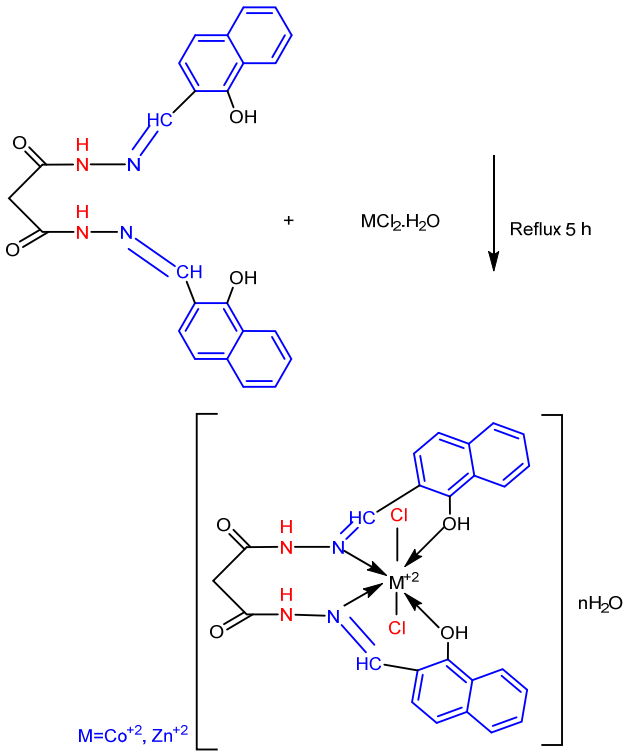

Scheme 3. Preparation of Schiff base metal complexes

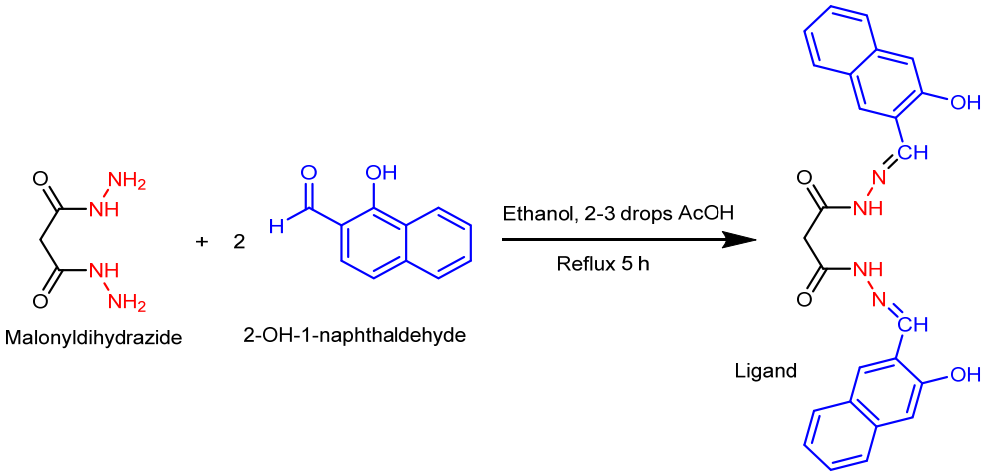

Scheme 2. Preparation of Schiff base ligand

product to create the target ligand, which was then recrystallized and further purified. Eventually, by reacting it with the appropriate metallic chloride, the obtained ligand was employed to create five new complexes. Table 1 lists the percentage yields and physical characteristics of the produced compounds. As will be discussed in more detail in the following sections, several methods were utilized to characterize the chemical structure of synthesized materials.

Characterization by Element Micro Analysis

Element micro analysis C, H, N, and X was performed, and it was discovered that the actual findings matched the theory, as given in Table 2. Metal salts were utilized in a 1:1 reaction of ligand and metal, and all of the complexes were determined to be non-electrolytes by their molar conductivities.

Characterization of Schiff Base Ligand by ^{1}H-NMR Spectroscopy

Using ^{1}H-NMR spectroscopy, the chemical composition of the produced ligand was examined. As a result, as shown in Fig. 1, the ^{1}H-NMR spectrum exhibits the necessary peaks at the appropriate habitats, integrations, and multiplicity to disclose the chemical structure of the ligand. Due to the structure's two symmetrical imine groups, the proton of the imine group (N=CH) produces a strong, crisp singlet signal at 8.43 ppm. At chemical shifts of 10.88 and 8.11 ppm, respectively, the exchange protons of NH and OH groups have displayed singlet peaks. Due to its proximity to the carbonyl group, which is responsible for the de-shielding of protons, it is assumed that the 10.88 ppm in question belongs to the NH group. On the other hand, the protons of aromatic areas exhibit peaks in the aromatic region with sufficient integration, which is between 7.15 and 7.69 ppm. Due to its proximity to two carbonyl groups, the CH_2 group finally displayed a singlet peak in the aliphatic region at 3.07 ppm. Given everything mentioned above, it can be concluded that the ligand has been effectively synthesized with a high degree of purity. Table 3 provides a summary of the synthesized ligand's ^{1}H-NMR data.

Characterization of Schiff Base Ligand by ^{13}C-NMR Spectroscopy

Using ^{13}C-NMR spectroscopy, the chemical composition of the produced ligand was identified. Hence, as shown in Fig. 2, the ^{13}C-NMR spectrum exhibits the necessary peaks at the appropriate habitats to illustrate the chemical structure of the produced ligand. The imine group's carbon atom N=CH produces a peak at 148.10 ppm, where Schiff base groups are the spouse. Nevertheless, because oxygen has a greater electronegativity than nitrogen, which results in more de-shielding, carbonyl groups exhibit a peak at 167.11 ppm. Nevertheless, there is still a peak at 157.37 ppm above the aromatic area, which may be due to aromatic

Table 1. The physical properties of the prepared compounds

Compound formula	Color	m.p. (°C)	M.Wt (g⁄mol)	Yield%
Ligand	Yellow	230–234	440.36	80
$[CoLCl_2]\cdot 2H_2O$	Brown	245–248	606.32	72
$[ZnLCl_2]\cdot H_2O$	Yellowish	242–246	594.75	83

Table 2. The Element micro analysis C, H, N, and X of the prepared compounds

	Calculated (Analysis)				
	C %	H %	N %	X%	M %
L	68.17	4.58	12.72	---	--
$C_{25}H_{20}N_4O_4$	(67.53)	(5.62)	((11.94)		
Complex Co	49.52	3.99	9.24	11.69	9.72
$[CoLCl_2]\cdot 2H_2O$	(50.30)	(3.05)	(8.79)	(10.53)	(10.16)
Complex Zn	50.49	3.73	9.72	11.92	10.99
$[ZnLCl_2]\cdot H_2O$	(49.65)	(3.09)	(10.69)	(12.73)	(11.01)

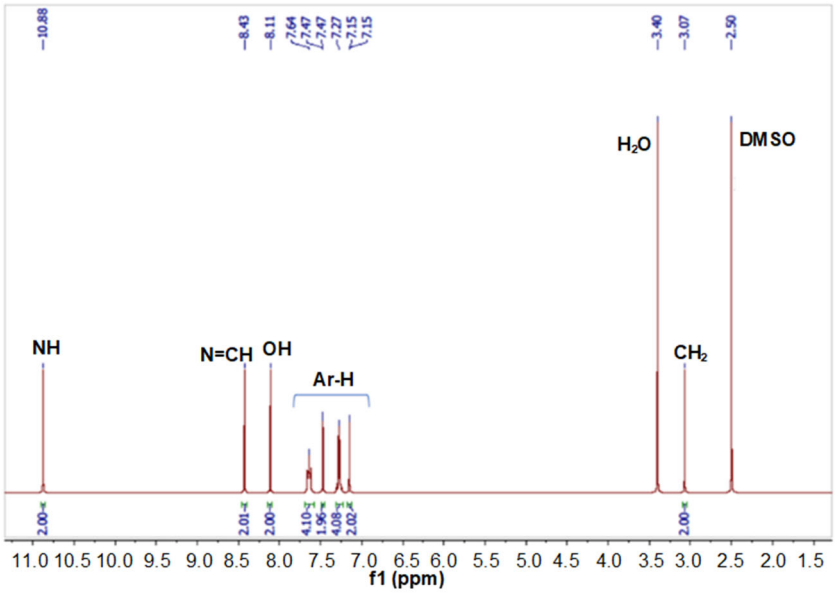

Fig 1. ^{1}H-NMR spectrum of synthesized ligand

Table 3. ^{1}H-NMR data of synthesized ligand

Compound	^{1}H-NMR
Ligand	δ/ppm = 3.07 (2H, CH_2), 7.15 (s, 2H, Ar-H), 7.20–7.32 (m, 4H, Ar-H), 7.47 (s, 2H, Ar-H), 7.60–7.69 (m, 4H, Ar-H), 8.11 (s, 2H, OH from the phenolic proton), 8.43 (s, 2H, HC=N azomethine), 10.88 (s, 2H, NH)

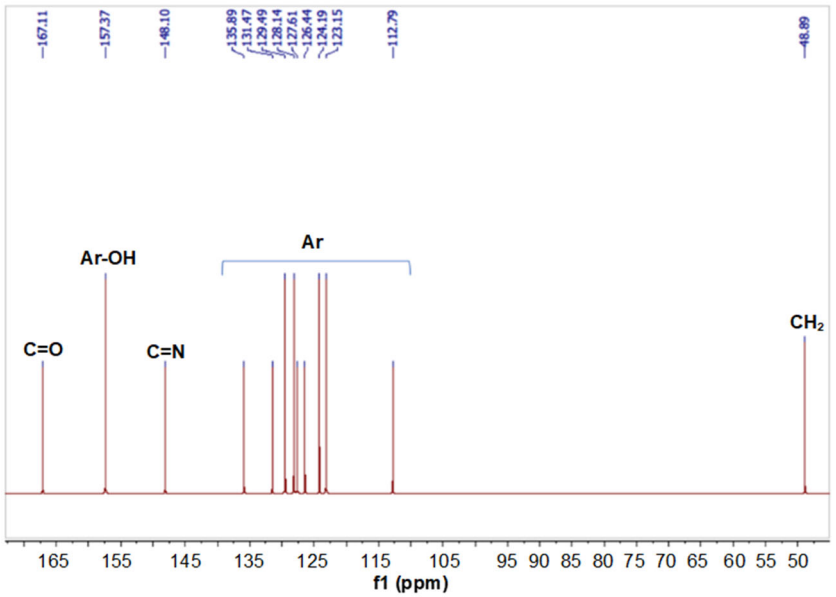

Fig 2. ^{13}C-NMR spectrum of synthesized ligand

carbon atoms positioned near oxygen. As a result, the aromatic area, which is between 112.79 and 135.89 ppm, exhibits nine peaks in the carbon atoms. Lastly, because it is located close to two carbonyl groups, the CH_2 group displayed a peak at 48.89 ppm in the aliphatic area. Given everything mentioned above, it can be concluded that the ligand has been effectively synthesized with a high degree of purity. Table 4 provides a summary of the

synthesized ligand's ^{13}C-NMR data.

Characterization of Schiff Base Ligand and Its Complexes by FTIR

In order to identify the functional groups and the development of new bands in the produced compounds, FTIR is a useful technique [19]. The complexes formed by the ligand and their FTIR spectroscopy data are shown in Table 5. The tetradentate Schiff base ligand exhibits a sharp band at 3109 and 1596 cm^{-1}, which are ascribed to ν(C–H)Ar and (C=C), respectively. Around 1613 cm^{-1}, the stretching band of the azomethine group was identified as a strong band. As a result of the nitrogen giving electrons to the partly full d-orbitals of the metal ions, the coordination of the metal ions to the nitrogen azomethine causes a shift-up in the frequency of the C=N value [20]. The complexes' FTIR spectra display distinctive lines at 1613–1623 cm^{-1}, indicating that the metal ions coordinate with the ligand through the nitrogen atom of the azomethine compound [21]. In the FTIR spectra of the ligands, a significant band at 3409–3479 cm^{-1} is produced by the stretching vibrations of the phenolic hydroxyl group. The broadness is due to intermolecular hydrogen bonding between the phenolic and azomethine groups. The far-infrared spectra of the complexes showed new stretching modes at 422–476, 526–611, and 312–314 cm^{-1}, which are attributed to M–N, M–O, and M–Cl, respectively [22]. These stretching modes provide evidence for the formation of bonds between the divalent metal ions and the nitrogen azomethine, hydroxyl group, and chloride, respectively. The results mentioned previously are displayed in Fig. S1 to S3.

Characterization of Schiff Bases Ligand and Its Complexes by UV-Vis

Electronic spectra of L and their complexes were recorded in DMF solution at room temperature in the range of 200–1100 nm. The obtained data were presented in Table 6. The UV-Vis spectra of the Schiff base base ligand revealed two strong intensity absorption peaks at 309 and 351 nm ascribed to intra-ligand π–π* and

Table 4. ^{13}C-NMR data of synthesized ligand

Compound	^{13}C-NMR
Ligand	δ/ppm = 48.89 (1C, CH_2), 112.79, 123.15, 124.19, 126.44, 127.61, 128.14, 129.49, 131.47, 135.89 (18C, Ar naphthalene), 148.10 (2C, CH=N azomethine group), 157.37 (2C, Ar-OH) and 167.11 (2C, C=O)

Table 5. FTIR spectroscopy measurements of ligand and their complexes

Symbol	O-H phenol	N-H	C-H Ar	C-H Alp	C=O	C=N	C=C	M-O	M-N	M-Cl
Ligand	3409	3330	3109	2889	1700	1613	1596	---	---	---
$[CoLCl_2]\cdot 2H_2O$	3479	3355	3110	2893	1702	1623	1598	611	422	314
Zn	3479	3359	3053	2925	1703	1620	1577	526	476	312

Table 6. UV-Vis spectroscopy measurements of ligand and molar conductivity of metal complexes

Compound	λ_{max} (nm)	Absorption (cm^{-1})	Assignments	μ_{eff} (B.M) Exp (Theory)	Molar Cond. Ohm^{-1} cm^2 mol^{-1}	Geometry
Ligand	309	32362.4	π→π*	-		
	351	28490.0	n→π*			
$[CoLCl_2]\cdot 2H_2O$	412	24271.8	C.T	3.36	18	Octahedral
	582	17182.1	$^4T_1g_F \rightarrow {}^4T1g_p$	(3.782)		
	640	15625	$^4T_1g_F \rightarrow {}^4A_2g_{(F)}$			
$[ZnLCl_2]\cdot H_2O$	410	24390.2	CT	Di	12	Octahedral
	435	22988.5	M→L			

n–π* transitions of azomethine and carbonyl, respectively [23]. Changes in the positions of absorption bands were observed in the spectra of the complexes indicating the coordination of the metal ions through the azomethine and hydroxyl phenol functional groups [24], Fig. S4. The electronic spectrum of the Co(II) complex in DMF gave bands about 412, 582, and 640 nm, respectively assigned to charge transfer and $^4T_1g_{(F)} \rightarrow {}^4T_1g_{(p)}$ and $^4T_1g_{(F)} \rightarrow {}^4A_2g_{(F)}$. The magnetic moment of 3.63 BM and the detected electronic spectrum of the Co(II) complex give the probability of the formation of high-spin octahedral geometry [25], Fig. S5. The electronic spectra of the d^{10} Zn(II) complex exhibited a charge transfer band at 410 and 435 nm [26], Fig. S6. The molar conductivities indicate that all the prepared complexes are non-electrolyte complexes.

Characterization of Schiff Base Ligand by Mass Spectroscopy

The molecular weight of the formed compound is calculated using the mass spectrum, and the fragmentation that belongs to the compound under investigation is identified. The mass spectra of the produced Schiff base ligand were in agreement with the suggested structural formula, $C_{25}H_{20}N_4O_4$. The predicted M^+ value (440.36), as shown in Fig. 3, is matched by the molecular ion peak, which was discovered at m/e 440, validating their formula weight for the ligand. As it was successively fragmented, new unique peaks for the ligand were visible in the mass spectra.

Examine How Well Synthesis Compounds Work as PS Photo Stabilizers

It is well known that aromatic compounds, in general, have a high capacity to absorb light across a broad range of the ultraviolet spectrum and transform it into harmless heat without changing the chemical composition of the medium's content. This decreases the medium's photolysis capacity, increases its age when used externally, and provides protection from sunlight [27-28].

Using this information as a foundation, several techniques were used to assess the efficacy of synthesis complexes as optical stabilizers for PS films, including measuring the increase in the intensity of active groups formed as a result of irradiation, estimating the percentage of weight loss, and researching the surface formation of polymeric films.

Use the FTIR Method to Examine the PS Photodegradation Rate

By monitoring FTIR spectra in the range of 400–4000 cm^{-1}, the PS polymer film's level of photodegradation was kept track of locating the wide hydroxyl band between 3500 and 3200 cm^{-1} and the carbonyl adsorption band C=O at 1720 cm^{-1}, which are created as a result of irradiating the films. Due to the presence of the unsaturated group in the chemical makeup

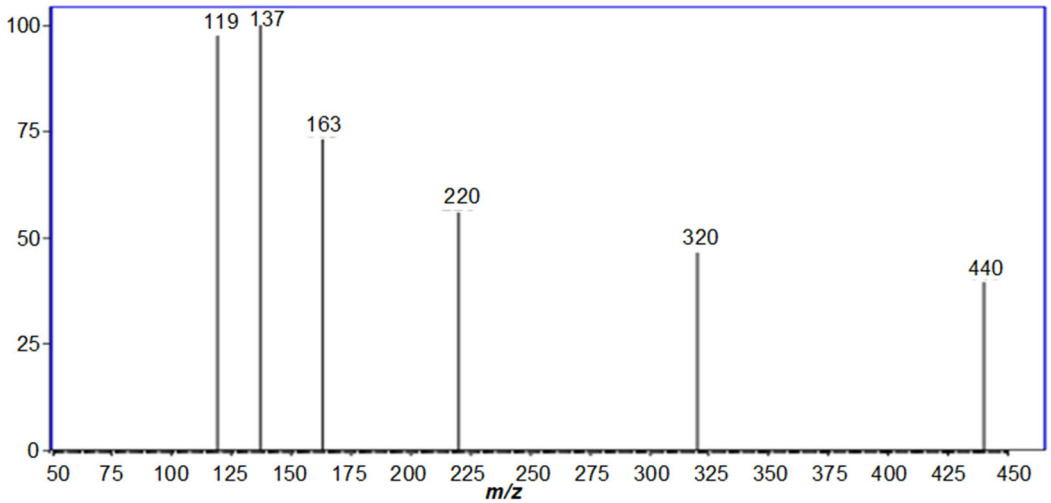

Fig 3. Mass spectrum of L

of the polymer and the difficulty in differentiating between them, the alkene group C=C was not followed up. Every 50 h of exposure time, changes in the carbonyl band C=O and hydroxyl OH intensity were seen, and Eq. (1) was applied as illustrated in Fig. S7 and S8. To track the growth in photolysis.

Accordingly, these beams were used to compare the absorption values of the standard absorption beam 1340 cm^{-1}, which is regarded as standard because it is unaffected by UV light, with the values of the standard absorption beam in order to determine the extent of polymer degradation during irradiation [29-30]. As a result, the absorbance (index) values of the hydroxyl and carbonyl groups were examined to assess the photodegradation, as illustrated in Fig. 4 and 5. The data and values in Tables 7 and 8 show that, in comparison to PS without additives, doping with synthesis complexes decreased the increasing rate of the I_{OH} and $I_{C=O}$ indices with increased irradiation duration. The conclusion is that all additives serve as optical stabilizers for PS films, with Co(II) complex serving as the most effective one.

Investigate the Photodegradation Rate of PS Using the Weight Loss Method

The percentage weight loss of the photodegraded PS films following irradiation was used to calculate the photo stabilization effectiveness of the synthesis complexes. This causes weight reduction, which is calculable using

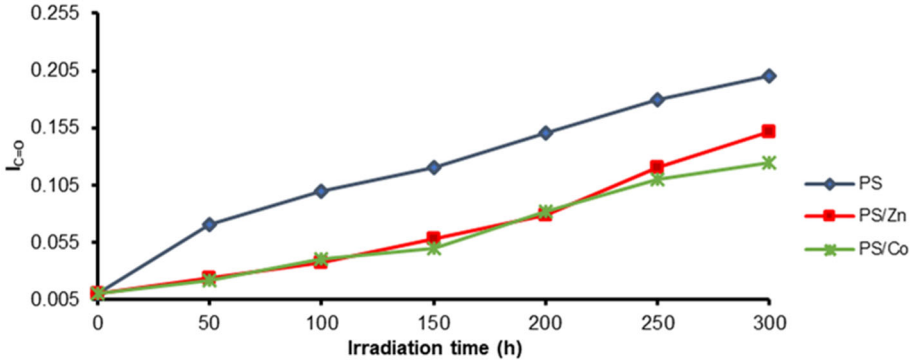

Fig 4. Index of carbonyl group $I_{C=O}$ for both pure PS and PS doped with stabilizers

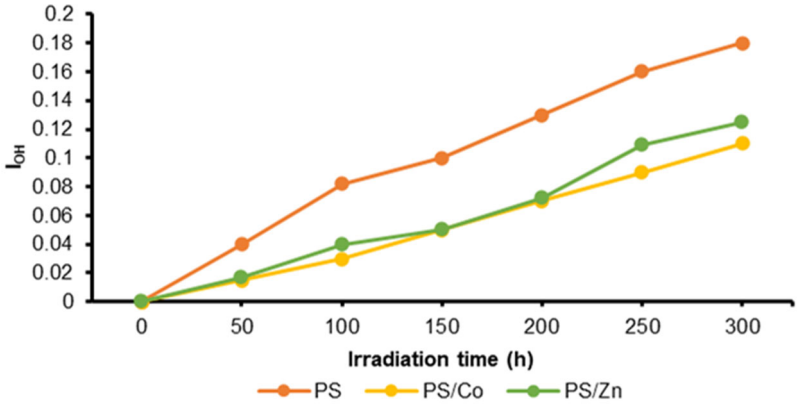

Fig 5. Index of hydroxyl group I_{OH} for both pure PS and PS doped with stabilizers

Table 7. $I_{C=O}$ data for pure PS and PS doped with stabilizers during the irradiation time

PS films	Irradiation time (h)						
	0	50	100	150	200	250	300
PS	0.010	0.070	0.100	0.120	0.150	0.180	0.200
PS/Zn	0.010	0.024	0.037	0.058	0.079	0.120	0.152
PS/Co	0.010	0.022	0.040	0.050	0.082	0.110	0.125

Table 8. I_{OH} data for both pure PS and doped PS during the irradiation period

PS films	Irradiation time (h)						
	0	50	100	150	200	250	300
PS	0	0.040	0.082	0.100	0.130	0.160	0.180
PS/Co	0	0.0150	0.030	0.050	0.070	0.090	0.110
PS/Zn	0	0.017	0.040	0.050	0.072	0.109	0.125

Eq. (2). Fig. 6 shows that when the irradiation period is increased, polystyrene steadily loses weight [31]. Nevertheless, compared to the undoped PS films, there was less weight loss in the doped PS films. The findings in Table 9 show that the cobalt complex was the most effective.

PS Stabilizing Study Using the Variance in the Average Molecular Weight

The primary chains of PS's polymeric structure are reportedly disrupted by photodegradation, which lowers the substance's average molecular weight [32]. The average molecular weight of PS after exposure to radiation is examined in this section, along with its differences from PS without additions. After being exposed to UV light, the PS solution's viscosity was measured, and the average molecular weight ($\overline{M}_v$) was determined. Using THF as a suitable solvent to dissolve the PS, the viscosity of the irradiation PS was evaluated using a viscometer at various time intervals. Fig. 6. plots the MV of PS vs the irradiation time. It is clear that the molecular weight decreases with longer irradiation times for both blank and mixed PS. The decrease for bare PS is, however, more severe than it is for PS that contains stabilizers Fig. 7 and Table 10.

Study of the Produced PS Films' Surfaces

The study of how polymer surfaces develop reveals details on the crystalline state, surface regularity, and flaws brought on by photons of light interacting with polymer molecules [33]. Based on this, the mechanism of photolysis and fission of the polymeric chains was identified. The surface morphology and stability of the polymers were also observed following exposure to UV light. Prior to and following irradiation, the surface formation of pure PS and PS doped with aromatic Schiff base complexes was investigated using SEM and AFM. It

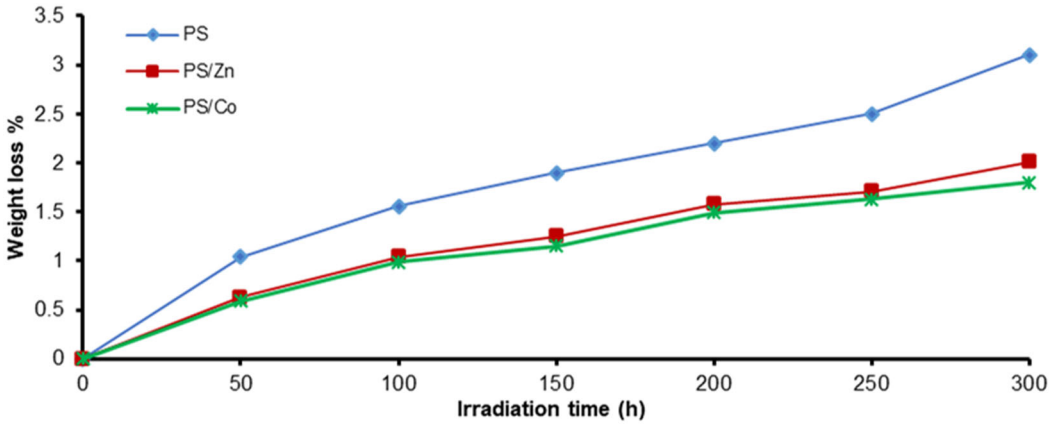

Fig 6. Weight loss % for both pure PS and PS doped with stabilizers

Table 9. Weight loss% data for both pure PS and doped PS during the irradiation period

PS films	Irradiation time (h)						
	0	50	100	150	200	250	300
PS	0	1.04	1.56	1.90	2.20	2.50	3.10
PS/Zn	0	0.63	1.04	1.25	1.58	1.71	2.01
PS/Co	0	0.59	0.99	1.15	1.49	1.63	1.80

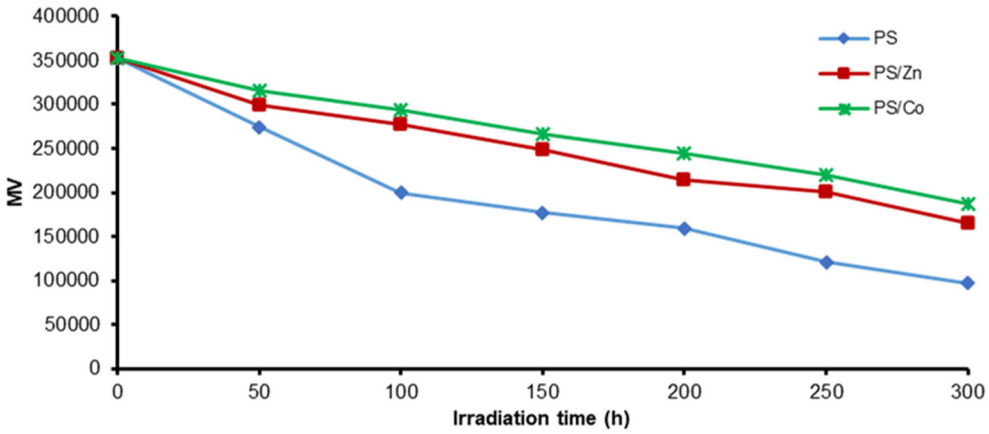

Fig 7. Average molecular weight for both pure PS and PS doped with stabilizers

Table 10. Effect of irradiation on the average molecular weight ($\bar{M}v$) of Ps films

PS Films	Irradiation time (h)						
	0	50	100	150	200	250	300
PS	352546	274355	200044	177254	159519	121284	96972
PS/Zn	353254	298685	277219	249244	214574	201154	165750
PS/Co	353244	315385	293219	266244	243874	220254	186650

provides crucial details on how radiation affects the PS surface.

Using Microscopic Images to Examine the Surface of PS Films

Prior research [34] demonstrated that before being exposed to radiation, the polymer's surface had a smooth texture and just a few small fractures. In contrast, the polymer's exposed surface exhibits photodegradation of the polymer chains in the form of many fractures, increased roughness, and a darker hue. This may be caused by the radiation's influence on tiny volatile pieces with a low molecular weight. The microscopic imaging method was utilized to acquire microscopic images of the PS films' surface following irradiation in order to monitor the deterioration of the films. The microscopic pictures of pure polystyrene before and after irradiation are shown in Fig. 8. Following 300 h of radiation exposure, the pictures demonstrate the formation of large black blotches, as illustrated in Fig. 8(b).

Fig. 10 displays microscopic images of synthetic material-doped polystyrene sheets. Little dark patches are seen on the film surfaces, notably for films doped with Zn complex, as shown in Fig. 9(a). The surfaces of the films are brighter and smoother when they are blended with the Co complex, as shown in Fig. 9(b). This demonstrates the efficiency of synthetic materials and their capacity to impede photodegradation by blocking the damaging effects of light on polystyrene films.

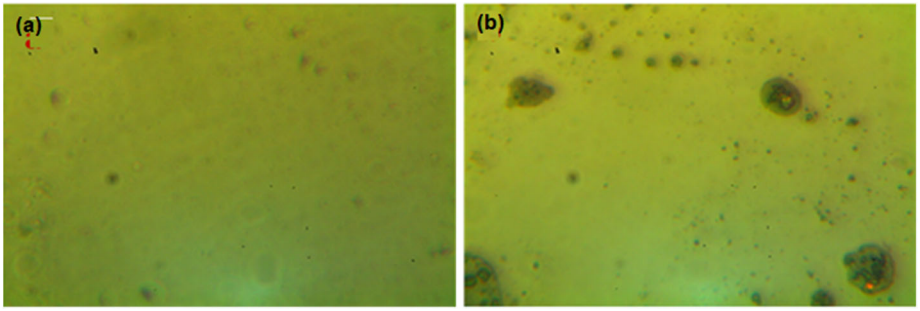

Fig 8. Microscopic images of blank PS film (a) before and (b) after irradiation

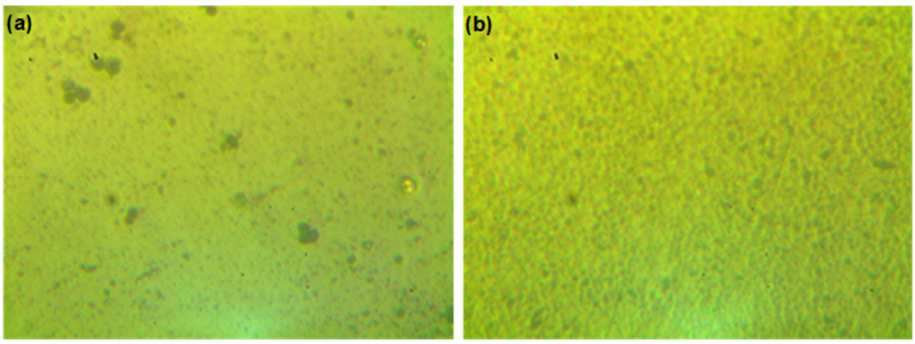

Fig 9. Microscopic images of blend PS films after irradiation (a) Zn(II) and (b) Co(II)

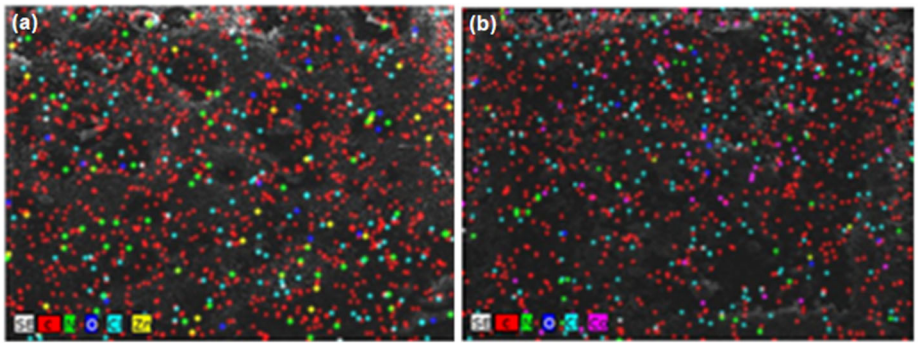

Fig 10. SEM-EDX mapping of blend PS films after irradiation (a) Zn(II) and (b) Co(II)

Energy Dispersive X-ray (EDX) Mapping with Scanning Electron Microscopy (SEM)

Using EDX mapping of doped PS films and SEM, the distribution of generated complexes on the polymeric surface was investigated. This method was utilized to provide specifics on the elemental composition of solid surfaces for PS films combined with synthetic chemicals [35]. It is common practice to use EDX in conjunction with SEM to determine the chemical composition of manufactured films. The SEM images and EDX mapping of doped films by those complexes, as shown in Fig. 10, illustrate the elemental makeup of the produced complexes and their homogenous distribution inside the polymeric chains.

An Atomic Force Microscope (AFM) Is Used to Display the Photostability of Polystyrene Films

The surface morphologies of PS films were investigated using the AFM method. Due to its ability to scan both two- and three-dimensional topography, it is an effective microscopy instrument for examining surface data at the nanoscale. AFM may be used to assess the PS surface's features and roughness. The root mean square roughness (Sq), one of the dispersion variables used to assess surface roughness, is derived by first square-rooting each height value in the dataset. Surface skewness is a measurement of the asymmetry of the surface's deviation from the mean plane. Radiation exposure to PS for an extended period of time causes a rough and cracked surface. Topographic AFM pictures of the surface of the PS films in two and three dimensions after 300 h of radiation exposure demonstrate that the root mean square (Rq) and roughness average have significantly risen, going from 0.639 nm (before radiation) to 2.35 nm (after radiation), as shown in Table 11. This is brought on by the photodegradation that radiation exposure causes to PS's chemical structure. Fig. 11 shows AFM images of untreated PS taken both before and after it was exposed to UV light.

In contrast, employing synthetic additives increased the surface roughness of PS following irradiation compared to untreated PS, as seen in Table 11. Hence, PS films with Co(II) doping exhibit the least

Table 11. Roughness data for blank and blended PS films

Films	Roughness average (nm)	Root mean square (Sq) (nm)
Blank PS before irradiation	0.639	0.956
Blank PS after irradiation	2.35	3.89
Zn(II)	2.33	3.29
Co(II)	1.99	2.52

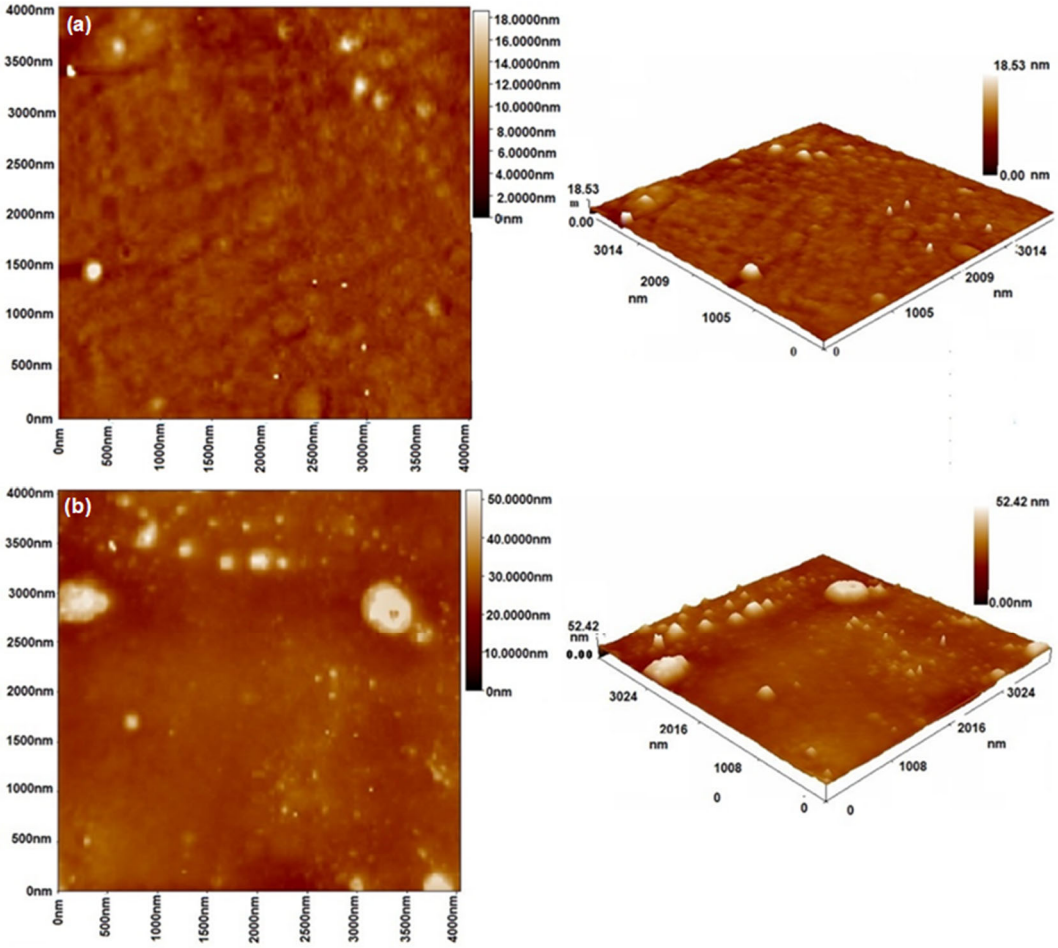

Fig 11. AFM images of PS films (a) before and (b) after irradiation at 300 h

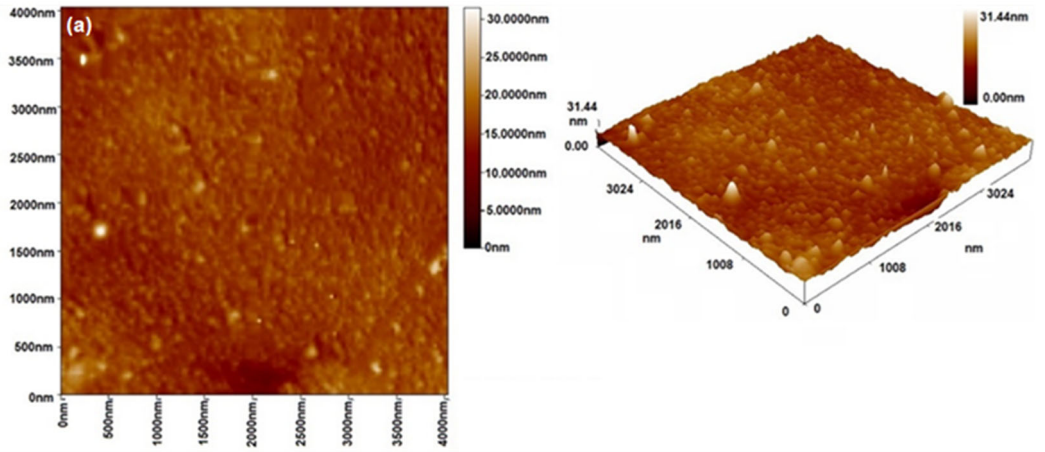

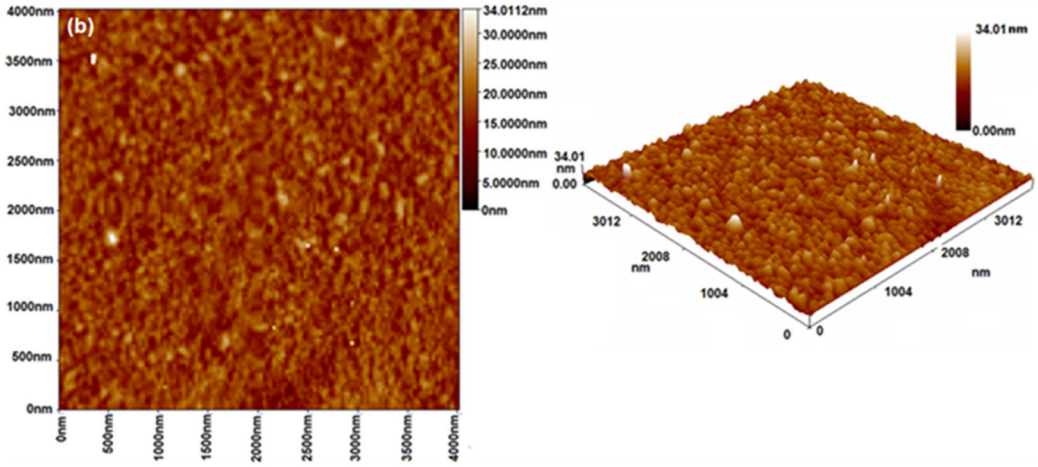

Fig 12. AFM images of blend PS films after irradiation (a) Zn(II) and (b) Co(II)

photodegradation and roughness, with Sq values of 2.52 nm. The addition of stabilizers significantly improved the photostability of PS films. Fig. 12 compares the irradiation-blended PS films with additives with the blank PS film in terms of surface homogeneity, smoothness, and roughness. In an AFM picture, the distance between peaks and valleys is frequently used as a proxy for surface roughness. The AFM technology uses this method to calculate the surface's roughness, which rises with distance. The Sq is believed to be more sensitive than the average roughness for large excursions from the mean line or plane. The PS film with cobalt complex doping had the lowest Sq value and roughness associated with photodegradation. Each of the aforementioned experiments supported this finding, showing that the cobalt complex is the best additive for PS-doped film to stop photodegradation. It is not totally clear what the reason is, therefore, more investigation may be required.

■ CONCLUSION

This work led to the effective synthesis of new Schiff base complexes, including Zn(II) and Co(II) complexes. In order to create pure target complexes, the malonyl dihydrazide had to first be combined with naphthaldehyde, and then it had to be reacted with the metal(II) chloride. The generated complexes were thoroughly characterized using FTIR, ^{1}H-NMR, ^{13}C-NMR, mass, and UV-Vis spectroscopies. In this study, a number of chemicals were used to photo-stabilize polystyrene (PS) and reduce the polymeric chains' photodegradation. The efficiency of the created complexes as photo-stabilizers was evaluated using a variety of techniques, including FTIR, weight loss, viscosity average molecular weight, light and AFM, SEM, and EDX mapping. These tests corroborated each other and demonstrated how effectively the new compounds stabilized PS pictures. They reduce the photodegradation of PS films containing these complexes compared to blank PS after 300 h of UV exposure. It has also shown the potency of the cobalt complex as a photo-stabilizer. These compounds' highly conjugated systems are to fault for this. As plastic waste constitutes a serious danger to the environment, particularly the marine ecosystem, the study's findings have significant implications for reducing PS usage globally.

■ SUPPORTING INFORMATION

Fig. S1 FTIR spectrum of Schiff Base ligand, Fig. S2 FTIR spectrum of Co(II) complex, Fig. S3 FTIR spectrum of Zn(II) Complex, Fig. S4 UV-Vis Spectra of ligand, Fig. S5 UV-Vis Spectra of Co(II) Complex, Fig. S6 UV-Vis Spectra of Zn(II) Complex, Fig. S7 FTIR spectrum of polystyrene before irradiation, Fig. S8 FTIR spectrum of polystyrene after irradiation.

■ ACKNOWLEDGMENTS

Thanks to Department of Chemistry, College of Science for Women, University of Baghdad, Iraq. To provide them with chemicals and research equipment.

■ AUTHOR CONTRIBUTIONS

Naser Shaalan conceived this idea, based on the expressions of Rehab Ghalib Hammoda supervised the project. Rehab Ghalib Hammoda carried out the experiment, wrote the manuscript, and performed the analysis. All authors discussed the results and contributed to the final manuscript.

■ REFERENCES

[1] Basha, M.H., Sulaiman, S.A., and Uemura, Y., 2020, Co-gasification of palm kernel shell and polystyrene plastic: Effect of different operating conditions, *J. Energy Inst.*, 93 (3), 1045–1052.

[2] Al-Mashhadani, M.H., Thamer, H., Adil, H., Ahmed, A., Ahmed, D.S., Bufaroosha, M., Jawad, A.H., and Yousif, E., 2021, Environmental and morphological behavior of polystyrene films containing Schiff base moiety, *Mater. Today: Proc.*, 42, 2693–2699.

[3] Wang, J., Wang, X., Zhao, S., Sun, B., Wang, Z., and Wang, J., 2020, Robust superhydrophobic mesh coated by PANI/TiO_2 nanoclusters for oil/water separation with high flux, self-cleaning, photodegradation and anti-corrosion, *Sep. Purif. Technol.*, 235, 116166.

[4] Zabaniotou, A., and Kassidi, E., 2003, Life cycle assessment applied to egg packaging made from polystyrene and recycled paper, *J. Cleaner Prod.*, 11 (5), 549–559.

[5] Wu, Y., Dong, L., Shu, X., Yang, Y., She, W., and Ran, Q., 2022, A review on recent advances in the fabrication and evaluation of superhydrophobic concrete, *Composites, Part B*, 237, 109867.

[6] Rabie, S.T., Ahmed, A.E., Sabaa, M.W., and Abd El-Ghaffar, M.A., 2013, Maleic diamides as photostabilizers for polystyrene, *J. Ind. Eng. Chem.*, 19 (6), 1869–1878.

[7] Liu, X., Sun, P., Qu, G., Jing, J., Zhang, T., Shi, H., and Zhao, Y., 2021, Insight into the characteristics and sorption behaviors of aged polystyrene microplastics through three type of accelerated oxidation processes, *J. Hazard. Mater.*, 407, 124836.

[8] Li, Y., Li, J., Ding, J., Song, Z., Yang, B., Zhang, C., and Guan, B., 2022, Degradation of nano-sized polystyrene plastics by ozonation or chlorination in drinking water disinfection processes, *Chem. Eng. J.*, 427, 131690.

[9] Khalaf, M., Fadhil, Z., Al-Mashhadani, M.H., Abdallh, M., Bufaroosha, M., Majeed, A., Salih, N., and Yousif, E., 2020, PVC films performance stabilized by dibutyltin(IV) complex for sustainable environment, *J. Phys.: Conf. Ser.*, 1664, 012072.

[10] Ahmed, A., Al-Mashhadani, M.H., Ahmed, D.S., Ahmed, A.A., Yousif, E., and Yusop, R.M., 2021, Preparation of polymeric films containing Schiff base as UV-absorber with good resistance against UV-photoaging, *Biointerface Res. Appl. Chem.*, 11, 12743–12749.

[11] Al-Mashhadani, M.H., Salman, E.A., Husain, A.A., Abdallh, M., Bufaroosha, M., and Yousif, E., 2022, Utilizing organic aromatic melamine moiety to modify poly(vinyl chloride) chemical structure and micro CuO that plays an important role to enhance its photophysical features, *Indones. J. Chem.*, 22 (5), 1187–1194.

[12] Jima'a, R.B., and Shaalan, N., 2023, Synthesis, characterization, and biological activity of new metal ion complexes with Schiff base derived from 2-acetylthiophene and isatin, *Egypt. J. Chem.*, 65 (132), 1409–1419.

[13] Ahmed, D.S., Mohammed, A., Husain, A.A., El-Hiti, G.A., Kadhom, M., Kariuki, B.M., and Yousif, E., 2022, Fabrication of highly photostable polystyrene films embedded with organometallic complexes, *Polymers*, 14 (5), 1024.

[14] Fadhil, Z., Zageer, D.S., Faris, A.H., Al-Mashhadani, M.H., Ahmed, A., Hashim, H., and Yousif, E., 2022, Extracted lignin from oil palm empty fruit bunch as natural eco-friendly poly(vinyl chloride) photo-stabilizer, *Mater. Sci. Energy Technol.*, 5, 15–21.

[15] Jose, T.S., Rajesh, C., Puthukkara, P.A.R., Unnikrishnan, K.S., and Arun, K.J., 2021, Accelerated photodegradation of polystyrene by TiO_2-polyaniline photocatalyst under UV radiation, *Eur. Polym. J.*, 153, 110493.

[16] Zhang, X., Su, H., Gao, P., Li, B., Feng, L., Liu, Y., Du,

Z., and Zhang, L., 2022, Effects and mechanisms of aged polystyrene microplastics on the photodegradation of sulfamethoxazole in water under simulated sunlight, *J. Hazard. Mater.*, 433, 128813.

[17] Mahdi, S.A., Ahmed, A.A., Yousif, E., Al-Mashhadani, M.H., Ahmed, A., Hashim, H., and Jawad, A.H., 2022, New organic PVC photostabilizers derived from synthesised novel coumarine moieties, *Mater. Sci. Energy Technol.*, 5, 278–293.

[18] Ali, A.A., Karasu, B., Allazov, M.R., and Ilyasli, T.M., 2013, Synthesis and study of $Ce_xPr_xMg_{1-2x}Al_2O_4$ ceramic pigment by combustion method using malonic acid dihydrazide as fuel, *Int. J. Sci. Eng. Res.*, 4 (8), 1686–1690.

[19] Hussein, K.A., and Shaalan, N., 2022, Synthesis, characterization, and antibacterial activity of lanthanide metal complexes with Schiff base ligand produced from reaction of 4,4-methylene diantipyrine with ethylenediamine, *Indones. J. Chem.*, 22 (5), 1365–1375.

[20] Shaalan, N., Khalaf, W.M., and Mahdi, S., 2022, Preparation and characterization of new tetra-dentate N_2O_2 Schiff base with some of metal ions complexes, *Indones. J. Chem.*, 22 (1), 62–71.

[21] Shaalan, N.D., and Abdulwahhab, S., 2021, Synthesis, characterization and biological activity study of some new metal complexes with Schiff's bases derived from [*O*-vanillin] with [2-amino-5-(2-hydroxy-ohenyl)-1,3,4-thiadiazole], *Egypt. J. Chem.*, 64 (8), 4059–4067.

[22] Tazin, N., Ragole, V.D., and Wankhede, D.S., 2019, Facile one pot synthesis of tetraamide macrocyclic complexes using malonyldihydrazide and *p*-nitrobenzaldehyde at room temperature, *Inorg. Nano-Met. Chem.*, 49 (9), 291–296.

[23] Jimaa, R.B., and Shaalan, N., 2022, Synthesis, characterization and biological activity new metal ion complexes with Schiff's bases derived from 2-Acetylthiophene and Isatin, *Egypt. J. Chem.*, 65 (13), 1409–1419.

[24] Hussein, K.A., Mahdi, S., and Shaalan, N., 2023, Synthesis, spectroscopy of new lanthanide complexes with Schiff base derived from (4-antipyrinecarboxaldehyde with ethylene di-amine) and study the bioactivity, *Baghdad Sci. J.*, 20 (2), 469–482.

[25] Majeed, N.M., Abd. Al-Sahab, S., and Al Shemary, R.K., 2021, Eco-friendly and efficient composition, diagnosis, theoretical, kinetic studies, antibacterial and anticancer activities of mixed some metal complexes of tridentate Schiff base ligand, *Int. J. Pharm. Res.*, 13 (1), 3358–3369.

[26] Mohan, B., and Shaalan, N., 2023, Highly thermally stable and biologically active compounds prepared to be polymer stabilizers consisting of a Schiff base and its complexes derived from 2-hydroxynaphthaldehyde, *J. Med. Chem. Sci.*, 6 (2), 355–364.

[27] Alpay, A., Tuna, Ö., and Simsek, E.B., 2020, Deposition of perovskite-type $LaFeO_3$ particles on spherical commercial polystyrene resin: A new platform for enhanced photo-Fenton-catalyzed degradation and simultaneous wastewater purification, *Environ. Technol. Innovation*, 20, 101175.

[28] Xiao, L., Zhao, Y., Jin, B., Zhang, Q., Chai, Z., and Peng, R., 2020, Synthesis of novel ultraviolet stabilizers based on [60]fullerene and their effects on photo-oxidative degradation of polystyrene, *Fullerenes, Nanotubes Carbon Nanostruct.*, 28 (6), 465–473.

[29] Fakhri, L.A., Ghanbarzadeh, B., Dehghannya, J., Hosseini, M., and Dadashi, S., 2021, Photo-catalytic and biotic degradation of polystyrene packaging film: Effect of zinc oxide photocatalyst nanoparticles and nanoclay, *Chemosphere*, 283, 130972.

[30] Luna, C.B.B., Siqueira, D.D., Araújo, E.M., and Fook, M.V.L., 2020, Photodegradation of polystyrene/rubber waste blends compatibilized with SBS copolymer, *J. Elastomers Plast.*, 52 (4), 356–379.

[31] Yousif, E., Haddad, R., El-Hiti, G.A., and Yusop, R.M., 2017, Spectroscopic and photochemical stability of polystyrene films in the presence of metal complexes, *J. Taibah Univ. Sci*., 11 (6), 997–1007.
Mageed, Z.N., Kadhium, S.S., Rodhan, W.F., and Mohammed, H.H., 2022, Study of the photostabilization of polystyrene in the presence and absence of Schiff base derivatives, *Egypt. J. Chem*., 65 (4), 675–683.
[32] Fajstavr, D., Neznalová, K., Švorčík, V., and Slepička, P., 2019, LIPSS structures induced on graphene-polystyrene composite, *Materials*, 12 (21), 3460.
[33] Slepička, P., Neznalová, K., Fajstavr, D., and Švorčík, V., 2020, Nanostructuring of honeycomb-like polystyrene with excimer laser, *Prog. Org. Coat*., 145, 105670.
[34] Nguyen, T.N., Rangel, A., and Migonney, V., 2021, Fibronectin adsorption on polystyrene sulfonate-grafted polyester using atomic force microscope, *Biointerphases*, 16 (5), 051003.